Face-centred icosahedral Al - Mg - Li alloys: a free-electron quasicrystal

1997 J. Phys.: Condens. Matter 9 10725

(http://iopscience.iop.org/0953-8984/9/48/015)

J. Phys.: Condens. Matter **9** (1997) 10725–10738. Printed in the UK PII: S0953-8984(97)85833-X

Face-centred icosahedral Al–Mg–Li alloys: a free-electron quasicrystal

G Dell'Acqua†‡, M Krajčí†§ and J Hafner†

† Institut für Theoretische Physik, and Centre for Computational Materials Science, Technische Universität Wien, Wiedner Hauptstraße 8–10, A-1040 Wien, Austria

‡ Dipartimento di Fisica, Università degli Studi di Padova, I-35131 Padova, Italy

§ Institute of Physics, Slovak Academy of Sciences, SK-84228 Bratislava, Slovak Republic

Received 8 July 1997, in final form 8 September 1997

Abstract. We present detailed studies of the atomic and electronic structure of quasicrystalline Al–Mg–Li alloys. The face-centred icosahedral structure is described by decorating the even and odd twelvefold vertices of a canonical cell tiling with $Al_{24}Mg_{20}$ and $Al_{24}Li_{20}$ Bergman clusters, respectively. The electronic structure has been calculated using a real-space tight-binding linear muffin-tin orbital method. The electronic spectrum is characterized by a deep, structure-induced pseudogap just below the Fermi level and similar structures at higher binding energies associated with the face-centred icosahedral order.

1. Introduction

Ever since the discovery of quasicrystals [1] the question of why nature should prefer quasiperiodic to periodic order has been widely discussed. Very early it was pointed out [2–5] that the stoichiometry of many quasicrystalline alloys appears to be governed by a Hume-Rothery rule, placing the Fermi level into a minimum of the electronic density of states (DOS) (a 'pseudogap') induced by an effective Brillouin-zone boundary. Band-structure calculations for rational approximants to quasicrystals do indeed demonstrate the existence of a structure-induced DOS minimum in a number of icosahedral quasicrystals [6–11], and these predictions have been confirmed by various experimental techniques [12]. On the other hand both electronic structure calculations [13, 14] and photoelectron spectroscopy [15] agree that no DOS minimum at the Fermi level exists in decagonal quasicrystals‖, and that the stability of the decagonal phases is related rather to hybridization effects in the d bands of the transition-metal constituents than to a Hume-Rothery effect.

For the icosahedral alloys too, the existence of a Hume-Rothery-like pseudogap at the Fermi level must be seen in its context. (a) Although the DOS minimum seems to be a generic property of icosahedral quasicrystals, it is certainly not a specific property: it also exists in crystalline, amorphous, and even liquid phases of similar composition [9]. In the Al–Mn system for example, the Hume-Rothery minimum is much more pronounced in crystalline Al_6Mn than in the quasicrystalline phase [6, 14, 18]. (b) One also has to

‖ In a very recent paper [16] Stadnik *et al* re-analyse the photoemission data for decagonal Al–Cu–Co(Ni) alloys and argue that the decreasing slope of the density of states at the Fermi level is the result of a structure-induced DOS minimum superposed on a background with increasing slope. However, the detailed electronic structure calculations performed for this system [17] provide no justification for the assumption of such a background.

0953-8984/97/4810725+14$19.50

differentiate between the different classes of quasicrystal: simple icosahedral (SI) and face-centred icosahedral (FCI). In the thermodynamically stable FCI quasicrystals (Al–Cu–Fe, Al–Pd–Mn, Al–Pd–Re, ...) the d band of the transition-metal with the lower band filling overlaps with the Fermi level, so s, p–d and d–d hybridization effects have an important influence on the formation of a pseudogap [14, 18]. Among the SCI quasicrystals we have to distinguish between structures of the Mackay icosahedron type (e.g. i-Al–Mn) and Frank–Kasper triacontahedron-type quasicrystals (e.g. i-Al–Cu–Li, i-Al–Mg–Zn (Cu)). The valence band structure of the former class is again dominated by the d-electron states of the transition-metal constituents [6, 18]; this applies of course in particular to Ti-based quasicrystals [19]. The triacontahedron-type quasicrystals of the Al–Mg–Zn (Cu) and Al–Cu–Li (Mg) families on the other hand contain only simple metals and noble metals. Hence the valence band close to the Fermi level is dominated by s, p electrons and the structure-induced Hume-Rothery pseudogap is expected to have a decisive influence on the stability of the quasicrystalline phase.

For Al–Mg–Zn both electronic structure calculations [8, 9] and experiment (photo-electron spectroscopy and electronic specific heat measurements) [20] show that the electronic density of states at the Fermi level is reduced to about 70% of its free-electron value, both for the metastable $Al_{0.166}Zn_{0.462}Mg_{0.372}$ quasicrystal and for the crystalline Frank–Kasper compound $Al_{0.161}Zn_{0.444}Mg_{0.395}$ (the lowest-order rational approximant). The calculated DOS shows that there is almost no variation of the electronic spectrum in the hierarchy of the rational approximants—hence they all receive an equal amount of band-gap stabilization. From this point of view it is not surprising that stable 2/1 and 3/2 approximants have been reported [21, 22]. The quasicrystalline phase is stable in a narrow composition range around $Al_{0.15}Zn_{0.41}Mg_{0.44}$; in the metastable quasicrystals the Al content may varied between 13 and 25 at.% by substituting Al for Zn [20, 23]. In the Frank–Kasper phase the Al content may even be varied between 20.5 and 50.5 at.%, albeit at a slightly lower Mg content. With these concentrations, valence electron concentrations of $e/a = 2.15$ for the stable quasicrystal, $e/a = 2.13$–2.25 for the metastable icosahedral phases, and $e/a = 2.20$–2.50 for the Frank–Kasper phases are calculated. Photoemission spectra [20] indicate a slight broadening of the pseudogap at lower e/a ratios—this is in contrast to the trend expected from a simple filling of a rigid valence band. Hence the almost equal stability of quasicrystalline and approximant phases over a wide range of composition and valence electron concentration results from the interplay of size (packing) and electronic effects: at lower Mg concentrations ($\sim$39.5 at.%) ideal close-packing conditions are achieved in the $(Al, Zn)_{49}Mg_{32}$ Frank–Kasper phase, and this stabilizes the crystalline phase even at higher e/a ratios where the electronic contribution is small. Lower e/a ratios can be achieved only by increasing both the Zn and the Mg content: due to the substitution of the larger Mg atoms for the small Al atoms the packing becomes less favourable, but this is overcompensated by a more pronounced electronic effect. For a more detailed discussion we refer the reader to the paper by Takeuchi and Mizutani [20]. Evidently further detailed high-resolution studies of the electronic structure, both theoretical and experimental, are desirable.

The situation is similar in icosahedral and approximant Al–Cu–Li phases: self-consistent electronic structure calculations predict structure-induced pseudogaps at E_F for both the quasicrystal and the crystalline R phase (= the 1/1 approximant) [7, 10]. The DOS at E_F is predicted to be 7% lower in the quasicrystal than in the R phase. This is in good agreement with estimates based on nuclear magnetic resonance studies [24] and with photoemission [25] and soft-x-ray spectroscopy [26]. Almost identical structures have been proposed for the crystalline and icosahedral Al–Zn–Mg and Al–Cu–Li phases, based on the structure of

the Frank–Kasper phase proposed by Bergman *et al* [27] and its interpretation in terms of a decorated periodic Penrose tiling proposed by Henley and Elser [28]. However, since the Li content of Al–Cu–Li (32.5 at.% in the ideal R phase structure) is lower than the Mg content of Al–Zn–Mg (39.5 at.% in the ideal structure of the Frank–Kasper phase), some Mg sites in Al–Zn–Mg have to be occupied by Al and this leads to a less favourable packing, so electronic stabilization becomes more important.

Hence the general conclusion is that for this class of quasicrystalline and approximant structures the main stabilizing mechanism is—as proposed by Frank and Kasper decades ago [29]—based on the close packing of spheres of different sizes. The electronic Hume-Rothery mechanism plays an important role at compositions where the close-packing requirements can no longer be perfectly satisfied but where the criteria for the Fermi-surface/Brillouin-zone interactions are met.

The recent discovery of an icosahedral phase in the ternary Al–Mg–Li system [30, 31] suggests extending the studies of a possible Hume-Rothery-type stabilization of quasicrystals. The Al–Mg–Li quasicrystals are interesting for multiple reasons.

(i) The alloy consists only of s, p-bonded simple metals. Hence the structure of the valence band is expected to be closer to the free-electron limit than for Al–Zn–Mg and Al–Li–Cu where the hybridization of the s, p band with the Zn and Cu d states leads to a deformation of the valence band.

(ii) The diffraction data suggest that Al–Mg–Li possesses a face-centred icosahedral (FCI) structure which can be interpreted as an ordered superlattice of the Frank–Kasper triacontahedron-type SI structure. Hence Al–Mg–Li is the first transition-metal-free and the first triacontahedron-type FCI quasicrystal.

(iii) In both Al–Zn–Mg and Al–Cu–Li the distribution of Al/Zn and Al/Cu atoms is disordered whereas the idealized structure of Al–Mg–Li is perfectly ordered.

The present work is devoted to the investigation of the electronic structure of this new FCI Al–Mg–Li phase. For the lowest-order approximant we adopt the model proposed by Tsai *et al* [31] based on an ordered superlattice of the $(Al, Zn)_{49}Mg_{32}$ Frank–Kasper phase. Higher-order approximants are constructed via the canonical cell tiling (CCT) proposed by Henley [32] and applied by Mihalkovič and Mrafko [33] and Windisch *et al* [10] to describe the structure of i-Al–Cu–Li. The electronic structure of a hierarchy of approximants (up to 8/5) was calculated using a real-space tight-binding linear-muffin-tin-orbital method. The calculated DOS shows a deep structure-induced minimum at E_F and additional structures at higher binding energy reflecting the FCI superlattice order.

2. Atomic structure

The atomic structure proposed by Tsai *et al* [31] combines elements of the FCI structure proposed for icosahedral Al–Cu–Fe [34] with the decoration of the icosahedral vertices by Bergman clusters leading to the Henley–Elser model for the triacontahedron-type SI quasicrystals. A FCI structure is created by dividing the six-dimensional hypercubic lattice into two simple cubic lattices whose vertices have even or odd parities (defined in terms of the sum $n = \sum_i n_i$ of the six-dimensional indices $(n_1, n_2, n_3, n_4, n_5, n_6), n_i \in \mathbb{Z}$). The sites of the icosahedral lattice created by the projection on the three-dimensional space have the parity of their six-dimensional counterpart.

The building principle of the FCI Al–Cu–Fe phase is that of defining three different atomic surfaces in 6D space centred on the odd and even twelvefold vertices and on the body-centred (bc) positions. The atomic surface centred on the odd nodes is divided into

subshells, this division determining the local chemical order [34]. It has been pointed out that the structures created by the 6D refinement correspond to an average structure. In terms of a decoration of the vertices of the icosahedral lattice this corresponds to pseudo-Mackay and Bergman clusters, with partially incomplete inner shells (depending on the details of the atomic surfaces) [35, 11].

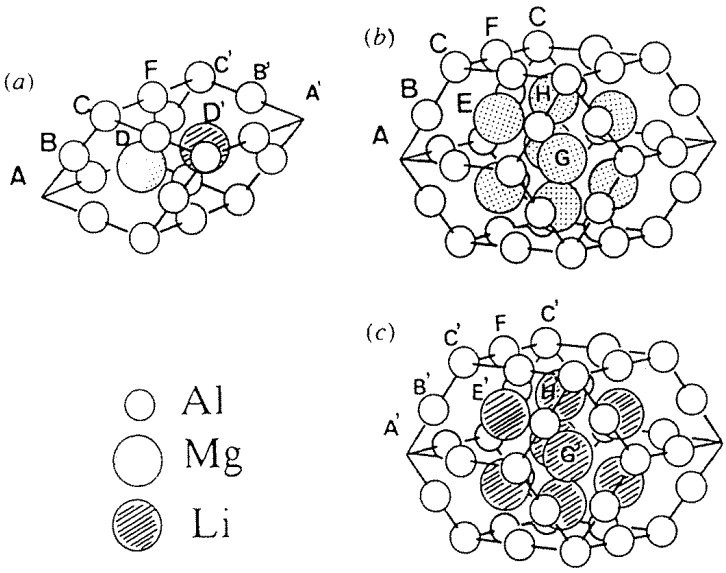

Figure 1. Modified Henley–Elser decoration for the prolate rhombohedron (*a*) and the rhombic dodecahedron (*b*), (*c*) located such that the long twofold axis connects two odd (even) twelvefold vertices; (*b*) and (*c*) define the nomenclature of the atomic sites in the $Al_{24}Mg_{20}$ and $Al_{24}Li_{20}$ Bergman clusters, respectively. After Tsai *et al* [31].

Our model for FCI Al–Mg–Li is not constructed via the projection method, but proceeds directly via a cluster decoration of the vertices of the icosahedral lattice. The constituent clusters are the $Al_{24}Mg_{20}$ and $Al_{24}Li_{20}$ Bergman clusters with the structure of rhombic triacontahedra. If the icosahedral lattice is decomposed into the oblate (OR) and prolate (PR) Penrose rhombohedra and, as a composite structural unit, a rhombic dodecahedron (RD) consisting of two ORs and two PRs, this leads to an atomic decoration very similar to that proposed by Henley and Elser [28] for SI Al–Mg–Zn: Al atoms occupy all vertices and midpoints of all edges of the structural units, except the vertices A, A′ (one even, the other odd) on the trigonal axes (see figure 1) which are vacant—this defines positions B, C, B′, C′ and F. A pair of Mg and Li atoms divides the long trigonal axis of the PR in the ratio $\tau{:}1{:}\tau$ (where $\tau = (1+\sqrt{5})/2$ is the Golden Mean), such that the Li atom (site D′) is close to the A′ vertex (see figure 1). The long twofold axis of a RD connects vertices of equal parity. Depending on the parity of these vertices, the positions in the interior of the RD are occupied by Mg or Li atoms: two Mg (Li) are placed again along the long trigonal axis of each of the two PRs (sites E, H and E′, H′, respectively; see figures 1(*b*), 1(*c*)). Two other E (E′) sites are introduced such that the decoration has a mirror symmetry with respect to a plane bisecting the long twofold axis, and finally two H (H′) sites are introduced along the short twofold axis such that the interior of each RD contains a slightly distorted hexagonal bipyramid of Mg (Li) atoms, depending on parity. With this decoration of the elementary units, $Al_{24}Mg_{20}$ and $Al_{24}Li_{20}$ Bergman

clusters are formed around the twelvefold A and A′ vertices. The Bergman clusters form the inner core of large 136-atom icosahedral clusters isomorphic to those identified in the Al–Cu–Li R phase and used to decorate the τ^3-inflated rhombohedra of the Audier–Guyot model [36].

In the quasicrystalline structures of the SI triacontahedron type there is no distinction between primed and unprimed sites (all twelvefold vertices are equivalent). In i-Al–Mg–Zn, sites A, B, C and F are occupied by Al (Zn), sites D, E, G and H by Mg. In i-Al–Cu–Li, sites A, B, C, F and H are occupied by Al (Cu), sites D, E and G by Li.

2.1. The 1/1 approximant

The unit cell of the 1/1 approximant has body-centred symmetry. Eight PRs are arranged along the body diagonal connecting the corners (positions A) and the centre (position A′) of the unit cell, and six RDs are placed with the long twofold axes along the cube edges. The space group symmetry is $Pm3$, i.e. a subgroup of $Im3$, the space group of the Al–Zn–Mg Frank–Kasper phase. The unit cell contains 160 atoms; the composition is $Al_{0.60}Mg_{0.20}Li_{0.20}$.

2.2. Higher-order approximants

For the construction of a hierarchy of periodic approximant structures approaching the quasicrystalline lattice one can either use the projection approach [37] (with the Golden Mean $\tau = (1+\sqrt{5})/2$ in the icosahedral basis in the perpendicular space replaced by the rational number $\tau_n = F_{n+1}/F_n$ (where the F_n are Fibonacci numbers, $F_{n+1} = F_n + F_{n-1}$)) to construct a periodic Penrose tiling (PPT) or the canonical cell tiling (CCT) proposed by Henley [32]. The canonical cells can be decomposed into the constituent OR, PR and RD elements of the Penrose tilings.

Table 1. The number of atoms, chemical composition, lattice constant and space group symmetry of rational approximants to quasicrystalline Al–Mg–Li.

τ_n	Number of atoms	Al (%)	Mg (%)	Li (%)	d_n (Å)	Symmetry
1/1	160	60	20	20	14.485	$Pm3$
2/1	680	61.18	19.41	19.41	23.437	$P2_13$
3/2	2888	62.05	18.98	18.98	37.922	$P2_13$
5/3	12 232	62.39	18.80	18.80	61.360	$P2_13$
8/5	51 816	61.80	19.10	19.10	99.282	$P2_13$

A detailed comparative study of higher-order PPT and CCT models for SI Al–Cu–Li has been presented by Windisch *et al* [38]. The higher-order CCT approximants have been constructed using a Monte Carlo method designed to optimize the density of 'b' and 'c' bonds running along the twofold and threefold symmetry axes of an icosahedron, respectively [33]. For the approximant PPTs constructed via the projection method, there is an additional degree of freedom associated with a shift of the acceptance domain in perpendicular space [39]. The important difference between the PPT and CCT is that the CCT preserves the large 136-atom icosahedral clusters around the twelvefold vertices at all levels of approximants, whereas the PPT in general does not, depending on the position of the acceptance domain. For a centrosymmetric position of the acceptance domain within the allowed range, the approximants up to $\tau \simeq 3/2$ are identical for the CCT and PPT, while differences appear for the higher-order approximants. The advantage of the CCT is

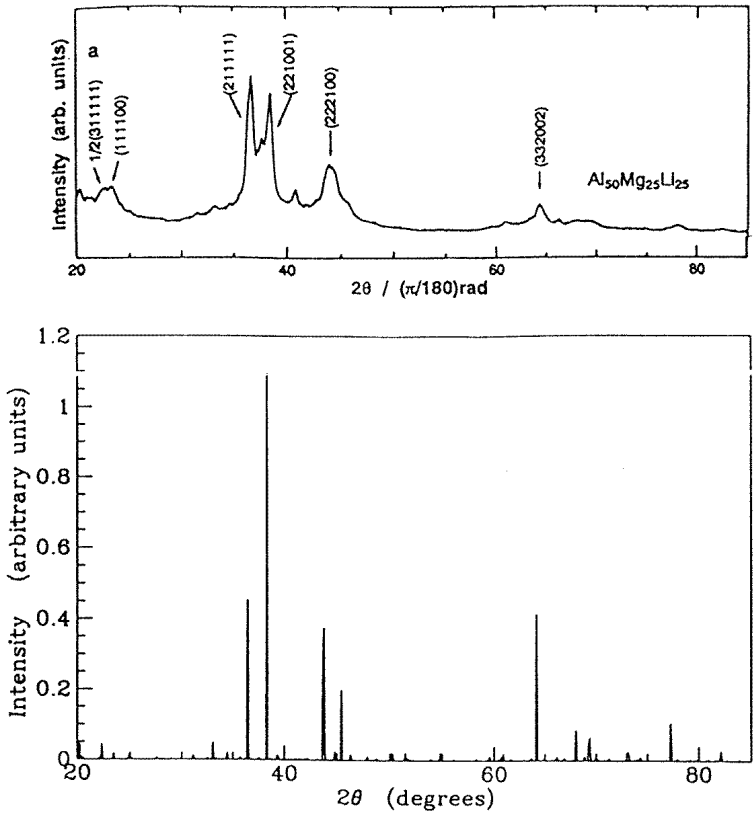

Figure 2. X-ray powder diffraction patterns for face-centred icosahedral Al–Mg–Li: top: experimental data of Niikura *et al* [30] for FCI $Al_{50}Mg_{25}Li_{25}$; bottom: as calculated for the 8/5 approximant with composition $Al_{62}Mg_{19}Li_{19}$ (cf. the text).

that it achieves the densest possible packing of these large icosahedral clusters whereas they are rather loosely packed in the PPT. In the present work we used CCT approximants up to $\tau \sim 8/5$. The characteristic properties of all of the approximants are summarized in table 1. The rhombohedral lattice constant is $a_R = 5.262$ Å, and the period of the nth-order approximant is given by

$$a_n = \sqrt{2 + 2/\sqrt{5}}\,\tau^n a_R.$$

For the lowest-order approximant the ideal composition is $Al_{60}Mg_{20}Li_{20}$, while for the higher-order approximants the composition converges quickly to the 'magic' value $Al_{\tau-1}Mg_{(1-\tau)/2}Li_{(1-\tau)/2} \sim Al_{0.618}Mg_{0.191}Li_{0.191}$. Experimentally, FCI quasicrystals with a composition $Al_{0.50}Mg_{0.25}Li_{0.25}$ have been prepared [30]. At the ideal composition Al occupies all sites with coordination numbers $Z = 12$ and $Z = 13$; the 13-fold-coordinated sites are located around the centre axes of the isolated oblate rhombohedra [40]. Mg and Li occupy the $Z = 14, 15, 16$ sites of the FCI lattice. For SI Al–Zn–Mg, Henley and Elser [28] proposed that a Mg content higher than that corresponding to the ideal chemical order could be realized by placing Mg on the $Z = 13$ sites. If we adopt this proposal for FCI Al–Mg–Li, the Al content is gradually reduced from $c_{Al} = 0.60$ in the 1/1 approximant (which does not contain any $Z = 13$ sites) to $c_{Al} = 0.565, 0.543, 0.517$ in the 2/1, 3/2

and 5/3 approximants respectively. However, this decoration leads to unfavourable Al–Mg (Li) distances: whereas the Al–Mg (Li) distances within the PR and RD units are $d_{\mathrm{Al-Mg\,(Li)}} = \tau^{-1}a_R \simeq 0.61a_R$, the shortest distance between a $Z = 13$ site and one of the $Z = 12$ sites is only $0.5a_R$, causing a considerable strain around the substitution sites. This strain could be resolved only by a local distortion of the lattice (which, however, has to preserve the overall icosahedral symmetry).

2.3. Comparison with experiment—atomic structure

Figure 2 compares the x-ray powder diffraction pattern calculated for the 8/5 CCT approximant with the experimental data of Niikura *et al* [30] for $Al_{0.50}Mg_{0.25}Li_{0.25}$. The diffraction peaks are indexed using Elser's method [41], considering the FCI phase as an ordered lattice. The FCI superstructure is characterized by the $\frac{1}{2}(311111)$ diffraction peak in the low-angle region which is absent in the SI phase. The agreement between the calculated and measured diffraction patterns is reasonably good, considering the difference in composition and the large width of the observed diffraction peaks. The strong peak broadening suggests that the FCI Al–Mg–Li phase possesses a highly disordered structure—possibly due to the high Mg and Li content.

The single-crystal diffraction pattern calculated for a plane containing the two-, three-, and fivefold symmetry axes is shown in figure 3. Part (a) displays the complete pattern calculated for the 8/5 approximant, and part (b) only the most intense peaks with those characteristic for the FCI phase marked by arrows, while part (c) shows for comparison the experimental pattern. The existence of these diffraction peaks confirms the similarity of the structure of i-Al–Mg–Li with those of i-Al–Cu–Fe and i-Al–Pd–Mn.

3. Electronic structure

Our calculation of the electronic structure of i-Al–Mg–Li is based on the strategy developed in our earlier work [8–11].

(a) For the 1/1 approximant the electronic structure is calculated self-consistently using the linear-muffin-tin-orbital (LMTO) method [42, 43].

(b) The LMTO Hamiltonian is transformed to the most-localized tight-binding basis. The TB-LMTO parameters are used to construct the TB Hamiltonian for the higher-order approximants.

(c) The total, partial and local densities of states and the Bloch spectral functions are calculated using the real-space recursion technique [44, 45].

The densities of states are calculated for starting vectors with random phases—four random vectors are used for the 3/2 approximant with 2888 atoms, while for the 8/5 approximant with 51 816 atoms a single starting vector is sufficient. To improve the resolution, the number of recursion levels is increased from 40 for the 3/2 to 80 for the 8/5 approximant. For further technical details we refer the reader to the earlier work.

3.1. The electronic density of states—Hume-Rothery stabilization

The total and local Al, Mg and Li densities of states calculated for the 3/2, 5/3 and 8/5 approximants are shown in figure 4; in addition the local s, p and d densities of states are shown in figure 5. The comparison of the DOS calculated for the hierarchy of approximants shows that at the level of the 5/3 and 8/5 approximants the electronic spectrum is essentially

(b)

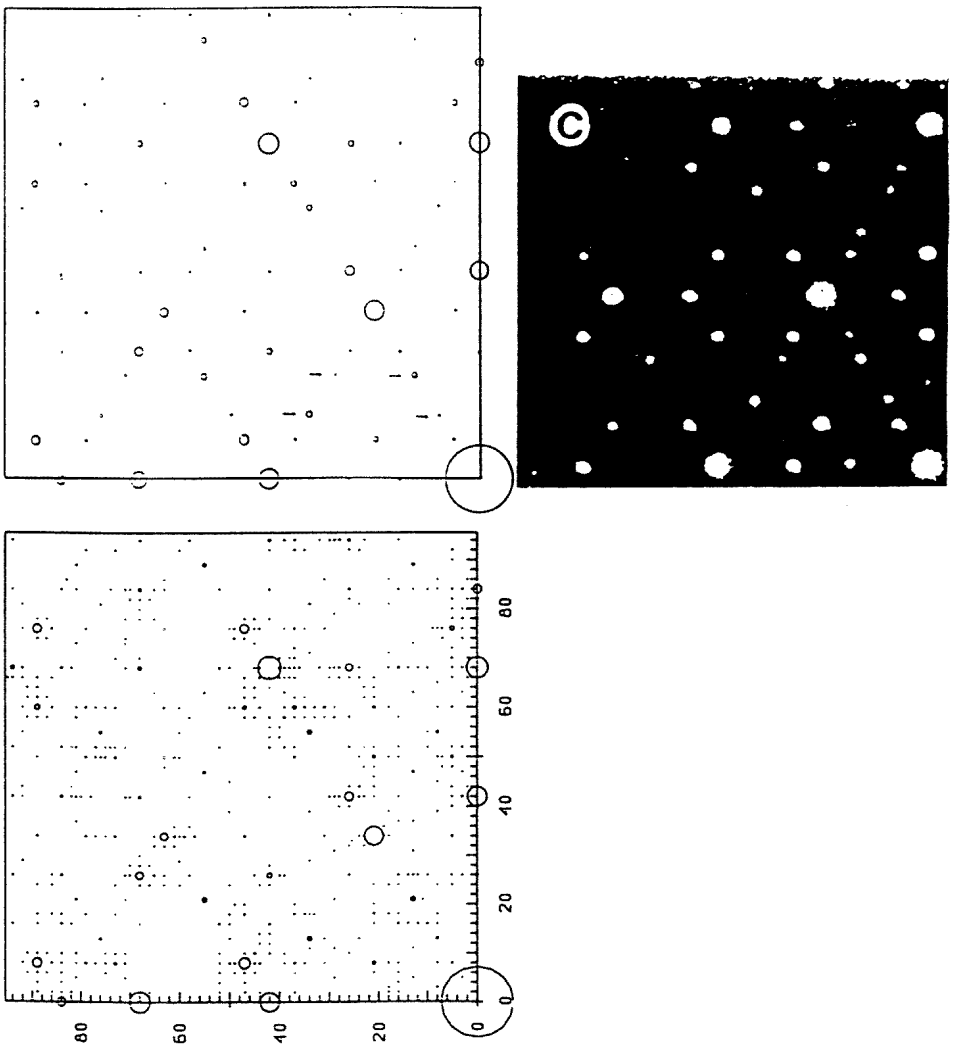

(a)

Figure 3. Single-crystal x-ray diffraction patterns of face-centred icosahedral Al–Mg–Li in a plane containing the two-, three-, and fivefold axes: (a) as calculated for the 8/5 CCT approximant; the components of the $\boldsymbol{k}$-vector are given in units of $2\pi/d$ where d is the lattice constant of the approximant; (b) the same pattern, but showing only the most intense peaks with the peaks characteristic for the icosahedral phase marked by arrows; and (c) the experimental diffraction pattern, after Niikura *et al* [30].

already converged to the quasiperiodic limit (at least within the resolution of $\sim$0.1 eV of the real-space recursion calculation; changes in the fine structure of the DOS can of course not be excluded). Except for the prominent DOS minimum just below the Fermi level, the form of the spectrum is very close to the free-electron parabola. The width of the occupied part of the valence band corresponds with $W = 9.3$ eV exactly to the free-electron value calculated

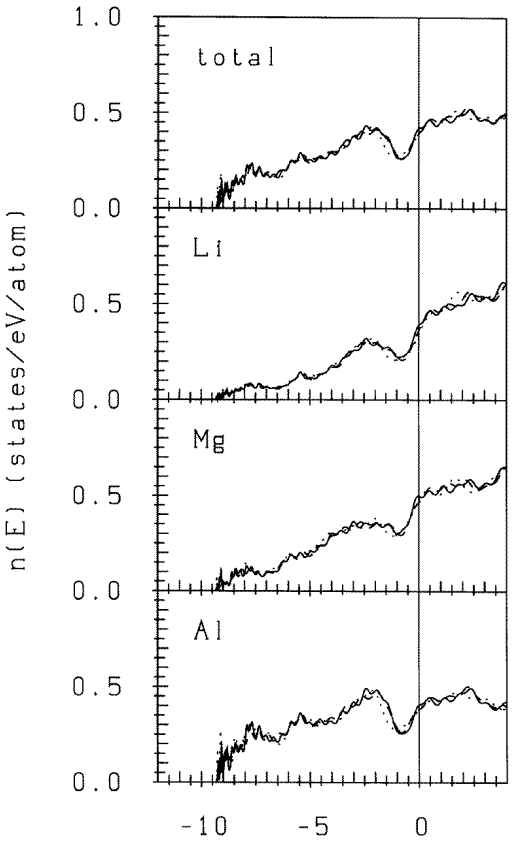

Figure 4. Total and local electronic densities of states for the 3/2 (dotted lines), 5/3 (dashed lines), and 8/5 approximants (full lines) to face-centred icosahedral Al–Mg–Li.

for the ideal composition $Al_{0.618}Mg_{0.191}Li_{0.191}$ (cf. table 1). The pseudogap close to E_F is induced by the (222100) Bragg peak whose wavenumber is almost equal to the diameter of the Fermi sphere. Other broad DOS minima appear at binding energies of $E \sim -4.7$ eV and $E \sim -6.8$ eV. The minimum at $E \sim -6.8$ eV is induced by the superstructure peaks $\frac{1}{2}(311111)$ and (111100)—although the corresponding Bragg peaks have only low intensity, the DOS minimum is quite pronounced because these small momentum transfers correspond to quite large pseudopotential form factors for all three components, especially for Al and Mg. Note that no corresponding DOS minima at high binding energies exist in the SI Frank–Kasper-type quasicrystals Al–Zn–Mg and Al–Cu–Li (see references [9, 10])—hence this DOS minimum can be considered as a manifestation of the FCI order in Al–Mg–Li. The most intense Bragg peaks (211111) and (221001) do not induce any structure in the DOS, because these wavenumbers fall close to a zero in the pseudopotential form factors. In this context it is interesting to have a look at the s-, p-, d-decomposed DOSs (see figure 5). For all three elements the s-electron DOS is concentrated in the lower half of the valence band while the p character dominates in the upper half of the band. The DOS minimum close to E_F is deep and narrow in the p-electron DOS, whereas the minimum in the s-electron DOS is much broader and also shifted to higher binding energies. This is a consequence of a quite strong nonlocality of the pseudopotentials of all three components: the s-electron

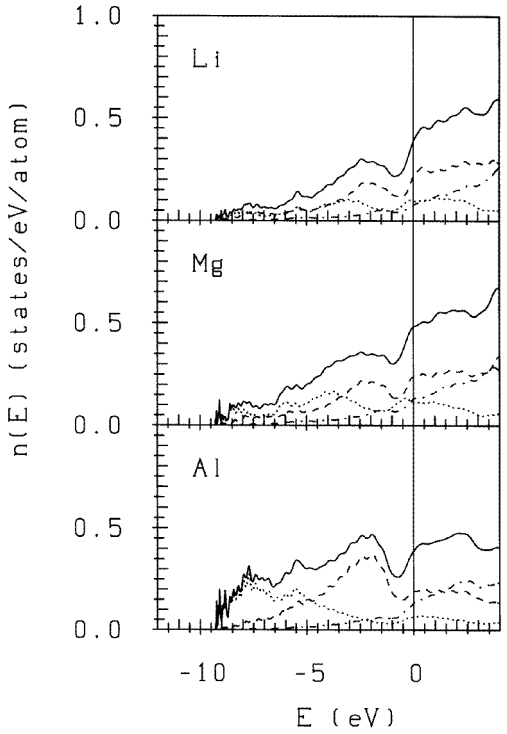

Figure 5. Angular-momentum-decomposed local electronic densities of states in face-centred icosahedral Al–Mg–Li: dotted: the s-electron DOS; dashed: the p-electron DOS; chain: the d-electron DOS; full lines: the local DOS.

pseudopotential is still quite large at the (221001) and (222100) Bragg peaks (at binding energies of ~ -2.5 eV and ~ -0.65 eV respectively), whereas a vanishing p-electron form factor suppresses the influence of the (221001) peak on the p DOS.

Exactly at the Fermi energy the total DOS is equal to the free-electron value of $n_{FE}(E_F) = 0.394$ states eV^{-1}/atom for the 5/3 approximant ($n(E_F) = 0.389$ states eV^{-1}/atom), and is even slightly enhanced for the 8/5 approximant ($n(E_F) = 0.432$ states eV^{-1}/atom). This indicates that at the composition where ideal packing can be achieved, the electron/atom ratio is, at 2.427 e/a, too high for achieving optimum band-gap stabilization. At the experimental composition $Al_{0.50}Mg_{0.25}Li_{0.25}$ the electron/atom ratio is reduced to 2.25 e/a, corresponding to a shift of the Fermi energy by 0.5 eV to lower energies. If a rigid-band model holds, this shift would place the Fermi level almost exactly at the minimum of the pseudogap.

However, calculations of the electronic DOS for the model placing Mg and Li atoms at the 13-fold-coordinated sites (and achieving almost the experimental composition; see section 2.2), show that for such a structure the rigid-band assumption is far from justified. The short Al–Mg (Li) distances in this structure model lead to the formation of localized bound states far below the bottom of the valence band. This indicates that the structure is locally unstable—future investigations will have to verify whether a local symmetry-conserving relaxation around the $Z = 13$ sites is sufficient to release the local strain created by the Al $\rightarrow$ Mg (Li) substitution and lead to a stable displacively modulated quasicrystalline structure.

3.2. Bloch spectral functions and quasiperiodic dispersion relations

The formation of a pseudogap in the electronic density of states is usually discussed in terms of the interaction of degenerate free-electron bands on an effective Brillouin-zone surface formed by the plane bisecting the wavevector of a prominent Bragg peak of the quasicrystalline lattice. Since in a quasicrystal the translational symmetry is broken and the wavevector is not a conserved quantity, this form of argument is not completely appropriate.

The proper way to generalize the Brillouin-zone argument to quasicrystals was pointed out by Niizeki and Akamatsu [46] and applied by us to the electronic structure problem [8–10]. A reciprocal lattice and Brillouin zones can be defined for the six-dimensional hypercubic lattice underlying the FCI lattice. The projections of the reciprocal-lattice vectors (the Γ points of the Brillouin zones in the extended zone scheme) and of the special high-symmetry (X, M, R, ...) points on the Brillouin-zone boundaries onto the three-dimensional wavenumber space defines sets of quasiperiodic Brillouin-zone centres (=Bragg peaks) and Brillouin-zone boundaries (=special points). Note that all special points are dense everywhere in $\boldsymbol{k}$-space, but their intensities are strongly modulated by interference effects. Hence the 'quasi-Brillouin-zone' structure is effectively discrete if only the more intense zone centres and special points are considered.

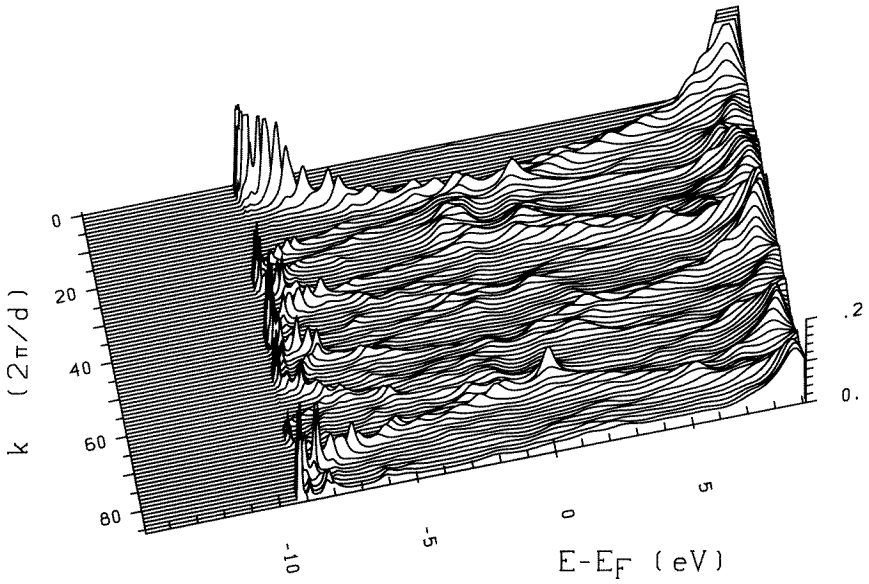

Figure 6. The Bloch spectral function $f(\boldsymbol{k}, E)$ for wavevectors oriented along a twofold symmetry axis, calculated for the 8/5 approximant to face-centred icosahedral Al–Mg–Li.

The usefulness of the quasi-Brillouin-zone concept becomes evident if we consider the electronic Bloch spectral functions $f(\boldsymbol{k}, E)$, i.e. the density of states projected onto plane waves with wavevector $\boldsymbol{k}$. For a crystal, the Bloch spectral function $f(\boldsymbol{k}, E)$ consists, for fixed wavevector, of a set of δ-functions at the eigenvalues of the Bloch states. Figure 6 shows the spectral function for $\boldsymbol{k}$-vectors oriented along a twofold symmetry axis, calculated for the 8/5 approximant to FCI Al–Mg–Li. Since the $\boldsymbol{k}$-vector is not a conserved quantity, the spectral function is a continuous function of energy. Nonetheless, dispersion relations $E(\boldsymbol{k})$ may be defined in terms of the peaks in the spectral functions. Figure 6 demonstrates

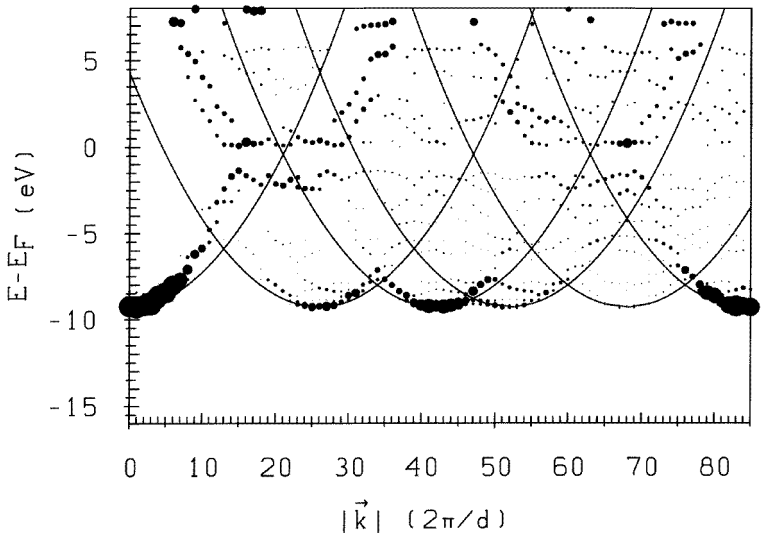

Figure 7. Dispersion relations $E = E_n(\boldsymbol{k})$ for electronic states in quasicrystalline Al–Mg–Li, derived from the positions of the peaks in the spectral function shown in figure 6. The size of each spot is proportional to the amplitude of the spectral function, and the solid lines show the free-electron parabolas centred at the most intense Bragg peaks located on the twofold axis; cf. the text.

that close to the bottom of the band the dispersion relations define a set of parabolic bands with their minima located at the intense Bragg peaks (=Γ points) along the twofold axis (cf. figure 3, but remember that the intensities are different for the x-ray diffraction pattern and for the geometrical structure factor, because of the weighting with the x-ray form factors). The complete dispersion relations along the twofold axis are shown in figure 7. One finds the following features.

(a) A set of dispersion relations following rather closely a free-electron parabola centred at the most intense Bragg peaks located on the twofold axis. Among those parabolic dispersion relations, the one with the origin at $|\boldsymbol{k}| = 26 \times (2\pi/d)$ is associated with a 'superlattice peak'.

(b) Where dispersion relations issuing from different Γ points cross, the interaction with the quasiperiodic lattice lifts the degeneracy.

(c) Close to the Fermi energy we identify a set of degenerate free-electron states; this leads to the formation of a pseudogap extending in $\boldsymbol{k}$-space, bounded by stationary states.

(d) A similar set of degenerate states exists at higher binding energies, leading to the other minima identified in the DOS. We confirm in particular that the minimum at $E \sim -6.8$ eV is associated with a superlattice reflection.

4. Summary and conclusions

We have performed an investigation of the atomic and electronic structure of the face-centred icosahedral Al–Mg–Li quasicrystal. We find that while the model proposed by Tsai *et al* [31] based on the decoration of the odd and even twelvefold vertices of the quasilattice with $Al_{24}Mg_{20}$ and $Al_{24}Li_{20}$ Bergman clusters leads to quite good agreement with the observed powder and single-crystal diffraction patterns, the composition $Al_{0.62}Mg_{0.19}Li_{0.19}$ differs

considerably from the composition of the most stable icosahedral phase, $Al_{0.50}Mg_{0.25}Li_{0.25}$. The possibility of substituting extra Mg and Li atoms at the 13-fold-coordinated Al sites has been explored.

The electronic structure of FCI Al–Mg–Li has been calculated for a series of higher-order rational approximants with up to $>50\,000$ atoms per cell. The electronic density of states is approximately parabolic, with a deep structure-induced DOS minimum close to the Fermi edge and weaker structures at higher binding energies. The mechanism for the formation of these pseudogaps has been examined within a generalized 'quasi-Brillouin-zone' formalism: the most intense Bragg reflections are the origins of free-electron dispersion relations. In the present case, one such set of free-electron-like states has its origin at a superlattice peak that exists only in the FCI structure, and not in the SI structure. The intersection of this 'band' with other free-electron bands occurs at higher binding energies and induces a local DOS minimum. This shows that the structures observed at higher binding energies are really induced by the face-centred superstructure of the Al–Mg–Li quasicrystals.

The fact that for the composition $Al_{0.62}Mg_{0.19}Li_{0.19}$ leading to ideal packing conditions the Fermi level falls at the upper edge of the pseudogap seems to suggest that the lower Al content of the laboratory-made quasicrystals might be explained within a rigid-band picture as due to an improved electronic stabilization. However, it turns out that the short Al–Mg and Al–Li distances introduced in the simple substitutional model lead to an unrealistic electronic structure. This confirms that Al $\rightarrow$ Mg (Li) substitution will be accompanied by local lattice distortions reducing the strain introduced by the substitution. These displacively distorted quasicrystalline structures will have to be examined in future studies.

Acknowledgments

G Dell'Acqua was supported by an ERASMUS grant of the European Union. The work at the TU Wien was supported by the Bundesministerium für Wissenschaft und Verkehr through the Centre for Computational Materials Science.

References

[1] Shechtman D, Blech I, Gratias D and Cahn J W 1984 *Phys. Rev. Lett.* **53** 1951
[2] Bancel P A and Henley C L 1986 *Phys. Rev.* B **33** 7917
[3] Friedel J and Denoyer F 1987 *C. R. Acad. Sci., Paris* II **305** 171
[4] Smith A P and Ashcroft N W 1987 *Phys. Rev. Lett.* **59** 1365
[5] Vaks V G, Kamyshenko V V and Samolyuk G D 1988 *Phys. Lett.* **132A** 131
[6] Fujiwara T 1989 *Phys. Rev.* B **40** 942
[7] Fujiwara T and Yokokawa T 1991 *Phys. Rev. Lett.* **66** 333
[8] Hafner J and Krajčí M 1992 *Phys. Rev. Lett.* **68** 2321
[9] Hafner J and Krajčí M 1993 *Phys. Rev.* B **47** 11 795
[10] Windisch M, Krajčí M and Hafner J 1994 *J. Phys.: Condens. Matter* **6** 6977
[11] Krajčí M, Windisch M, Hafner J, Kresse G and Mihalkovič M 1995 *Phys. Rev.* B **51** 17 355
[12] For a review see, e.g.,
Poon S J 1993 *Adv. Phys.* **41** 303
[13] Krajčí M, Hafner J and Mihalkovič M 1996 *Europhys. Lett.* **34** 207
[14] Krajčí M, Hafner J and Mihalkovič M 1997 *Phys. Rev.* B **55** 843
[15] Stadnik Z M, Zhang G W, Tsai A P and Inoue A 1995 *Phys. Lett.* **198A** 237
Stadnik Z M, Zhang G W, Tsai A P and Inoue A 1995 *Phys. Rev.* B **51** 11 358
[16] Stadnik Z M, Purdie D, Garnier M, Baer Y, Tsai A P, Inoue A, Edagawa K, Takeuchi S and Buschow K H J 1997 *Phys. Rev.* B **55** 10 938
[17] Krajčí M, Hafner J and Mihalkovič M 1997 *Phys. Rev.* B **56**

[18] Trambly de Laissardière G, Nguyen Manh D, Magaud L, Julieu J P, Cyrot-Lackmann F and Mayou D 1995 *Phys. Rev.* B **52** 7920
[19] Krajčí M and Hafner J 1994 *Europhys. Lett.* **27** 147
[20] Takeuchi T and Mizutani U 1995 *Phys. Rev.* B **52** 9300
[21] Edagawa K, Naito N and Takeuchi S 1992 *Phil. Mag.* **65** 1011
[22] Mukhopadhyay N K, Isihara K N, Ranganathan S and Chattopadhyay K 1991 *Acta Metall.* **39** 1151
[23] Takeuchi T, Murasaki S, Matsumoto A and Mizutani U 1993 *J. Non-Cryst. Solids* **156–158** 914
[24] Hippert F, Kandel L, Calvayrac Y and Dubost B 1992 *Phys. Rev. Lett.* **69** 2086
[25] Bruhwiler A, Wagner J L, Biggs B D, Shen Y, Wong K M, Schnatterly S E and Poon S J 1988 *Phys. Rev.* B **33** 6529
[26] Matsubara H, Ogawa S, Kinoshita T, Kishi K, Takeuchi S, Kimura K and Suga S 1991 *Japan. J. Appl. Phys.* **30** L389
[27] Bergman G, Waugh J L T and Pauling L 1957 *Acta Crystallogr.* **10** 254
[28] Henley C L and Elser V 1986 *Phil. Mag.* B **53** L59
[29] Frank F C and Kasper J C 1958 *Acta Crystallogr.* **11** 184
Frank F C and Kasper J C 1959 *Acta Crystallogr.* **12** 483
[30] Niikura A, Tsai A P, Inoue A, Masumoto T and Yamamoto A 1993 *Japan. J. Appl. Phys.* **32** L1160
[31] Tsai A P, Yamamoto A, Niikura A, Inoue A and Masumoto T 1994 *Phil. Mag. Lett.* **69** 343
[32] Henley C L 1991 *Phys. Rev.* B **43** 993
[33] Mihalkovič M and Mrafko P 1993 *Europhys. Lett.* **21** 463
[34] Cornier-Quiquandon M, Quivy A, Lefebvre S, Elkaim E, Heger G, Katz A and Gratias D 1991 *Phys. Rev.* B **44** 2071
[35] Elser V 1996 *Phil. Mag.* B **73** 641
Elser V 1997 private communication to M Mihalkovic and M Krajčí
[36] Audier M and Guyot P 1990 *Quasicrystals* ed T Fujiwara and T Ogawa (Berlin: Springer) p 181
[37] Bak P 1986 *Phys. Rev. Lett.* **56** 861
[38] Windisch M, Hafner J, Krajčí M and Mihalkovič M 1994 *Phys. Rev.* B **49** 8701
[39] Krajčí M and Hafner J 1992 *Phys. Rev.* B **46** 10 669
[40] Hafner J and Krajčí M 1993 *Phys. Rev.* B **47** 1084
[41] Elser V 1985 *Phys. Rev.* B **32** 4892
[42] Skriver H L 1984 *The LMTO Method* (Berlin: Springer)
[43] Šob M, Jepsen O and Andersen O K 1988 *Z. Phys. Chem.* **155** 515
Andersen O K, Jepsen O and Šob M 1987 *Electronic Band Structure and its Applications (Springer Lecture Notes in Physics 238)* ed M Yussouff (Berlin: Springer)
[44] Haydock R, Heine V and Kelly M J 1978 *J. Phys. C: Solid State Phys.* **8** 2591
[45] Heine V 1980 *Solid State Physics* vol 35, ed H Ehrenreich, F Seitz and D Turnbull (New York: Academic) p 1
[46] Niizeki K and Akamatsu T 1990 *J. Phys.: Condens. Matter* **2** 2758